Matter

CellPress

Article

Revealing Molecular Mechanisms in Hierarchical Nanoporous Carbon via Nuclear Magnetic Resonance

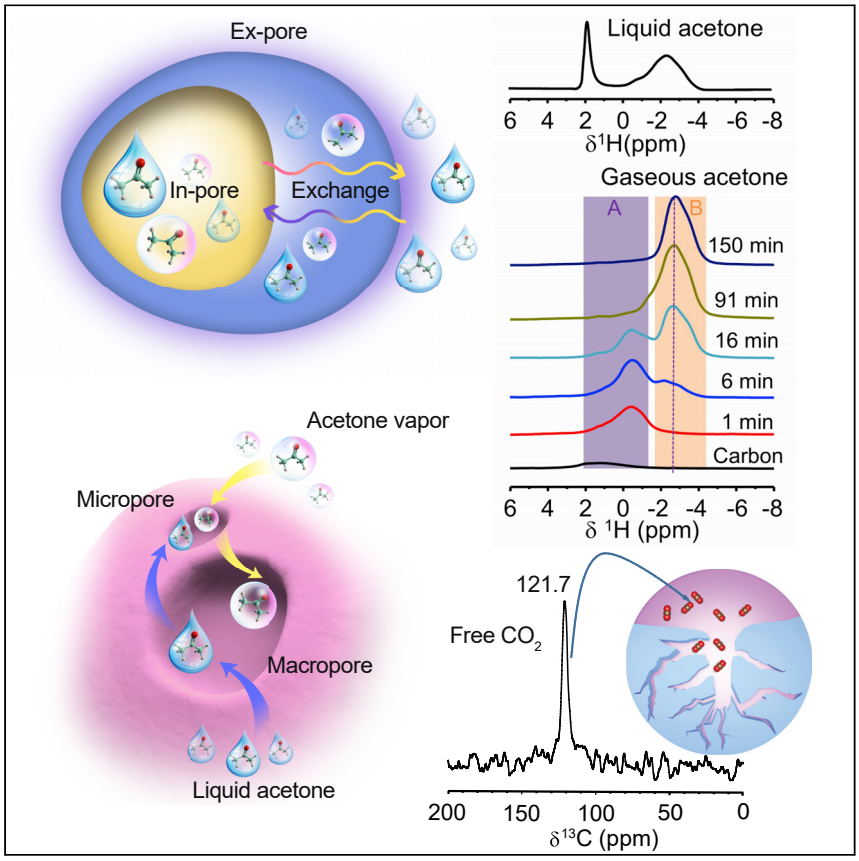

We synthesized hierarchical nanoporous carbons from wood, which exhibit Murray's law multiscale structures. We probe a molecular-scale study of adsorbate adsorption via nuclear magnetic resonance (NMR). Acetone vapor adsorption results show NMR chemical-shift changes with time, suggesting initial adsorption into mesopores, followed by diffusion into micropores. Schroeder's paradox is demonstrated by differences in observed shifts for adsorbed liquid vis-à-vis vapor phase in these carbons. These hierarchical nanoporous carbons show high CO_2 adsorption capacity, portending applications to carbon capture.

3 **Understanding**
Dependency and conditional studies on material behavior

Haiyan Mao, Jing Tang, Jun Xu, ..., Zhiyi Lu, Yi Cui, Jeffrey A. Reimer

yicui@stanford.edu (Y.C.)
reimer@berkeley.edu (J.A.R.)

HIGHLIGHTS

Fabricated a hierarchical nanoporous carbon following Murray's law by microwave heating

Probed a molecular-scale study of adsorbate adsorption via nuclear magnetic resonance

Provided an efficient way to quantitate adsorption of adsorbate in hierarchical carbons

Demonstrated presence of Schroeder's paradox by differences in liquid and vapor phase

Mao et al., Matter 3, 2093–2107
December 2, 2020
https://doi.org/10.1016/j.matt.2020.09.024

Matter

CellPress

Article

Revealing Molecular Mechanisms in Hierarchical Nanoporous Carbon via Nuclear Magnetic Resonance

Haiyan Mao,[1,8] Jing Tang,[2,7,8] Jun Xu,[1] Yucan Peng,[2] Jun Chen,[2] Bing Wu,[1] Yuanwen Jiang,[3] Kaipeng Hou,[4] Shuo Chen,[5] Jiangyan Wang,[2] Hye Ryoung Lee,[2] David M. Halat,[1,6] Bing Zhang,[4] Wei Chen,[2] Ariel Z. Plantz,[1] Zhiyi Lu,[2] Yi Cui,[2,7,*] and Jeffrey A. Reimer[1,6,9,*]

SUMMARY

Hierarchical nanoporous carbons (HNC) have been proven to be an effective adsorbent for the adsorption of volatile organic compounds (VOCs) and CO_2. However, questions remain regarding the hierarchical structure regulation, the adsorption mechanisms of adsorbate uptake, and interactions within the HNC. We synthesize HNC from wood, using a microwave-induced heating method incorporating K_2CO_3 activation. Our HNC exhibit Murray's law multiscale structures, prompting a molecular-scale study of adsorbate adsorption via nuclear magnetic resonance (NMR). NMR chemical shifts are consistent with ring-current effects from the adsorbent. Our NMR technique provides a convenient way to quantitate adsorption of adsorbate in HNC. VOC vapor adsorption results show NMR chemical-shift changes with time, suggesting initial adsorption into mesopores, followed by diffusion into micropores. Schroeder's paradox is demonstrated by differences in observed shifts for adsorbed liquid vis-à-vis vapor phase in these HNC. These HNC show high CO_2 adsorption capacity, portending applications to carbon capture.

INTRODUCTION

Volatile organic compounds (VOCs) are common air pollutants, contributing to the formation of ground-level ozone and carcinogens, known to be harmful to human health.[1] Carbon dioxide (CO_2) is the primary anthropogenic source of greenhouse gases that have affected the earth's biosphere, especially in the form of climate change.[2] The rational design of renewable, multidimensional, and microscopic materials for the adsorption of VOCs and CO_2 is therefore an important objective in functional materials research.[1,3,4] In particular, porous materials with nanosized pores play essential roles in the science and technology of VOCs and CO_2 adsorption and separation.[5,6] Nanoporous carbons derived from biomass are particularly promising due to their cost-efficient scalable fabrication, sustainable sourcing, high surface area, and microporous dominated structure.[7–9] Typically, adsorption in such nanoporous carbon is determined by physical adsorption (via van der Waals forces) and, ultimately, by micropore filling and capillary condensation.[10,11] Mesopores play a critical role by providing transport channels for the adsorption and desorption of molecules as well as additional adsorption sites.[12,13] We therefore focus our attention on VOC and CO_2 adsorption within sustainable, manufacturable[14] and hierarchically structured nanoporous carbons, which exhibit a panoply of pore sizes.

Various synthetic methods have been developed for hierarchically nanoporous carbons (HNC). Still, many methods suffer from lack of structural control, harsh synthesis

Progress and Potential

Hierarchical nanoporous carbons combining pore sizes of different length scales are highly important for separation processes. However, critical questions remain regarding the hierarchical structure regulation and the molecular mechanisms of gaseous adsorbate uptake and interactions within the hierarchical nanoporous carbons. These materials present characterization challenges in that there are no experimental techniques that can elucidate the molecular mechanisms of the organic compounds and CO_2 within the materials. We deployed multidimensional solid-state nuclear magnetic resonance (NMR) to generate maps of guest-framework interactions as a function of adsorbate concentrations and adsorption times. The NMR spectra provide insight toward the design of effective hierarchical pore structures. Our materials show a high volatile organic compounds/CO_2 physisorption capacity, which reveals promising application to carbon-capture strategies to mitigate global warming.

conditions, poorly degrading scaffolds, and unsuitable pores (e.g., clogged pores and beaded holes).[15–18] Inspired by plant structures, Murray's law materials have recently garnered attention, owing to the ability to regulate pore diameters from macroscopic to microscopic dimensions.[19,20] Nevertheless, progress in synthesizing Murray's law materials remains slow, hindered by the consistent bottleneck issues within the interconnected pores. Here, we synthesize HNC derived from pinewood that follows Murray's law of interconnected micro- and mesopores, using a microwave-induced method incorporating K_2CO_3 activation (Figure 1A).[21,22]

Several characterization methods have been used to investigate HNC's adsorption performance, such as adsorption capacity measurements via breakthrough experiments and gas adsorption isotherms.[23–26] The interactions between adsorbed molecules and the carbon pores are important factors during the adsorption process and cannot be revealed by bulk methods.[27] Solid-state nuclear magnetic resonance (NMR) is well suited to probe both local microscopic structure and the dynamical properties of guest compounds, which are confined in hierarchical porous carbons.[28,29] To date, NMR has been utilized to probe adsorbed molecules' environment into porous carbon-based host materials,[26] with applications in supercapacitors,[29,30] adsorption,[30] and hydrogen storage[31] materials. These studies led us to investigate hierarchical carbon materials by employing a combination of proton NMR and adsorption isotherm measurements.

We compare solid-state NMR studies of three typical liquid and gaseous VOCs as adsorbates, namely acetone, toluene, and *n*-hexane, as well as CO_2. These molecules were chosen because they are representative of environmental pollutants, with each molecule possessing different dimensions and polarity. We observe that the VOCs' adsorption from the liquid phase reflects uptake into the mesopores of HNC. The resulting chemical shifts show the effects of polyaromatic ring currents from the carbon adsorbent in all adsorbates. Integrating the NMR signals from liquid-adsorbed VOCs yields VOC mass uptakes that compare favorably with those determined by adsorption experiments. In an apparent manifestation of Schroeder's paradox, we found a difference in the observed NMR chemical shifts of VOCs obtained by gas-phase exposure and those obtained by liquid-phase exposure.[32] Finally, CO_2 physisorbed into HNC with surprising capacity. Together, these findings offer detailed insights into the interactions between liquid/gaseous adsorbates and HNC via NMR.

RESULTS AND DISCUSSION

Physicochemical and Structural Characteristics

The argon adsorption-desorption isotherm at 77 K of HNC is demonstrated in Figure 1B and Table S1. After microwave heating and K_2CO_3 activation, we observe that at relative pressure (P/P_0) below 0.05, the argon uptake increases sharply with the increase in relative pressure, proving the existence of microporous pore-dominated structure. These adsorption isotherms are close to type-I to -IV hybrid shape defined by the BDDT (Brunauer-Deming-Deming-Teller) classification.[33]

After the K_2CO_3/microwave treatment, the specific surface area by BET (Brunauer-Emmett-Teller) measurement and total pore volume of our HNC were remarkably improved (Table S1). The micropore surface area significantly rising from 30 to 1,857 m^2/g, with the micropore volume of biochar increasing from 0.016 to 0.741 cc/g, indicating that the micropores developed in the mesopore walls while some mesoporous channels collapsed. The development of porosity is associated

[1]Department of Chemical and Biomolecular Engineering, University of California, Berkeley, CA 94720, USA

[2]Department of Materials Science and Engineering, Stanford University, Stanford, CA 94305, USA

[3]Department of Chemical Engineering, Stanford University, Stanford, CA 94305, USA

[4]Department of Chemistry, University of California, Berkeley, CA 94720, USA

[5]Department of Physics, University of California, Berkeley, CA 94720, USA

[6]Materials Science Division, Lawrence Berkeley Laboratory, Berkeley, CA 94720, USA

[7]Stanford Institute for Materials and Energy Sciences, SLAC National Accelerator Laboratory, 2575 Sand Hill Road, Menlo Park, CA 94025, USA

[8]These authors contributed equally

[9]Lead Contact

*Correspondence: yicui@stanford.edu (Y.C.), reimer@berkeley.edu (J.A.R.)

https://doi.org/10.1016/j.matt.2020.09.024

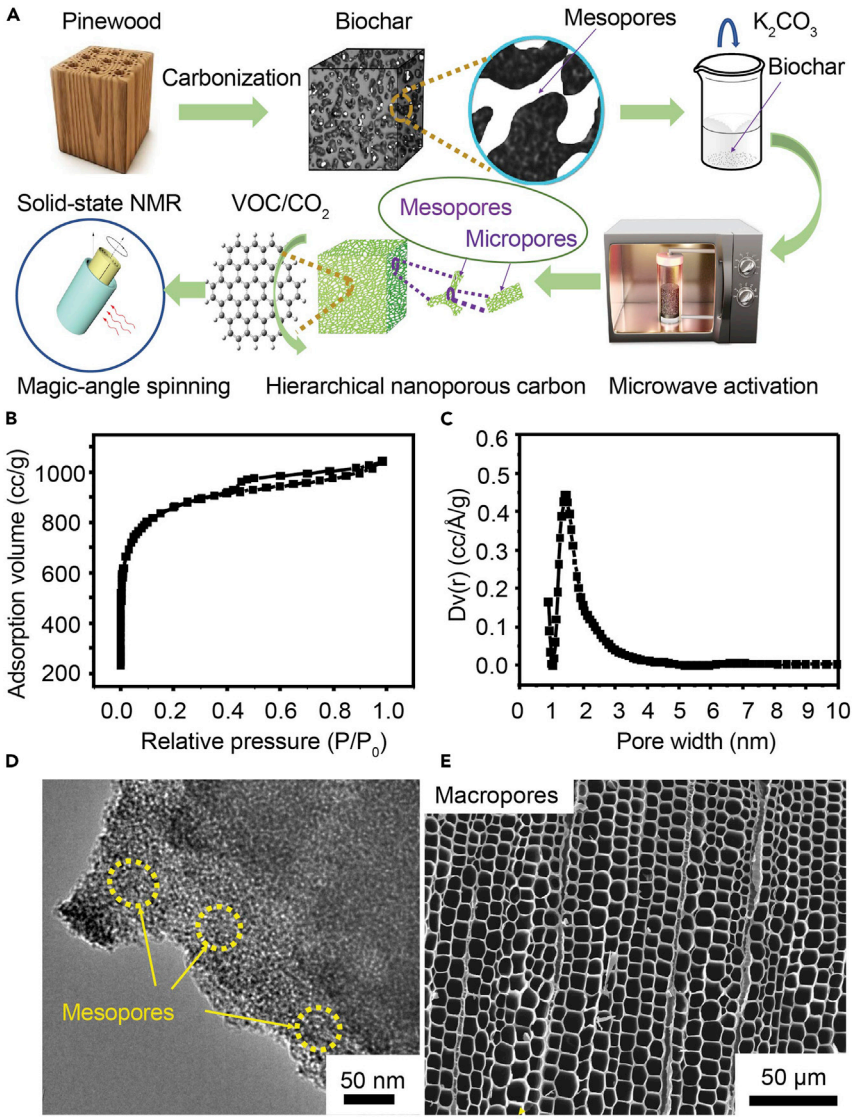

Figure 1. Preparation and Physical Characterization of HNC

(A) Schematic diagram of the fabrication process and characterization of the HNC.

(B) Argon adsorption isotherm of HNC at 77 K.

(C) Pore size distribution of HNC.

(D and E) Images of the HNC framework via (D) TEM and (E) SEM.

with the reaction of K_2CO_3 and C, which leads to the formation of K_2O, K, CO, and CO_2, whereby the high microwave temperature is assumed to accelerate the activation reaction.[34] The potassium species formed during the activation step diffuse into the internal structure of the biochar matrix, which widens existing pores and creates new ones. Consequently, the presence of K_2CO_3 promotes the formation of dominant micropores, a small fraction of mesopores, a much larger surface area, and a larger pore volume. The measured surface areas are 3.4 times higher than those of carbons activated by K_2CO_3 via thermal heating of samples derived from tobacco stem.[35]

The pore-size distribution curves plotted in Figure 1C are derived from argon adsorption measurements using the Horváth-Kawazoe method,[36] indicating that

HNC manifest a wide pore-size distribution covering micropores (0.65–2 nm) and mesopores (2–50 nm). The overwhelming majority of pore sizes include micropores (<2 nm), supermicropores (0.7–2 nm), and even ultramicropores (<0.7 nm). Overall, these isotherms (Figure 1B) reveal a micropore distribution with a mean size of 0.8 nm (D_{micro}). The K_2CO_3/microwave-activated HNC appear to follow Murray's law with three layers of the structure at the micro-, meso-, and macropore level, as well as abundant interconnected pores. Such a hierarchical pore structure aids in the diffusion of adsorbates and enhances the adsorption and desorption performance of the HNC.

The transmission electron microscopy (TEM) image (Figure 1D) also shows a disordered hierarchical nanoporous structure containing mesopores. The large quantities of white spots between the disordered carbon layers suggest that abundant mesopores exist in the HNC from pinewood. Using an auto-threshold function (Figure S1), we transformed the real-space images to binary images to clearly observe wormhole-like pores, as well as the interconnectivity of micropores and mesopores. A representative scanning electron microscopy (SEM) image of HNC is depicted in Figure 1E. The perfect honeycomb structure and prismatic rectangular cells from the natural pinewood are maintained after chemical activation. The dimensions of the cells were ca. 20 μm, and the wall thickness was ca. 2 μm. It is important to note that there was no evidence of rupture of the pinewood pore walls, indicating that the wall material had a sufficient tensile strength to impregnate K_2CO_3 and remove dissolved K_2CO_3. Upon K_2CO_3/microwave activation, the pores were etched and developed during the reaction of K with carbon. The result is similar to previously published SEM images of carbonized and activated virgin cork.[37,38] The present K_2CO_3/microwave activation of pinewood yields an interconnected HNC following Murray's law via a facile, inexpensive, and environmentally friendly process.

Adsorption of Liquid Acetone in Hierarchical Nanoporous Carbons

As shown in Figure 2A, proton (^{1}H) spin-echo magic-angle spinning (MAS) NMR was performed to obtain spectra of HNC loaded with acetone for the range 23 wt % to 141 wt %. The initial adsorption gives rise to a broad signal at −2.5 ppm. This signal was shifted from the signal for liquid acetone (2.2 ppm) to −2.5 ppm by 4.7 ppm and was assigned to "in-pore" acetone (Figure 2B). This shift to lower frequency results from ring currents emanating from the aromatic rings of the graphene planes in the pore walls.[39] This has previously been confirmed experimentally on micro- and mesoporous carbon.[39] The ring-current effect is strongly dependent on the distance between the NMR-observed nucleus and the center of the aromatic ring.[40,41]

Upon increasing the acetone loading, the broad line grows in intensity until it reaches a plateau at higher loadings (63 wt %), suggesting pore-filling and saturation. As the loading level increases to 82 wt %, a narrower peak appears at 1.8 ppm, a shift close to that of the methyl protons in neat acetone. This peak is associated with liquid acetone external to the HNC pores assigned to "ex-pore" acetone (Figure 2B). The chemical-shift deviation between the in-pore resonance and neat acetone is quantified by $\Delta\delta = \delta_{in-pore} - \delta_{neat}$, and has a value of −4.5 ppm (corresponding to the two peaks in Figure 2A at 141%).

To quantitate the exchange between the in-pore and ex-pore environments,[41] we conducted two-dimensional ^{1}H homonuclear exchange experiments[42] at various mixing times (0.001, 0.1, and 0.25 s). The results are shown in Figures 2C–2E. As expected, the cross peaks appearing at mixing times in excess of 0.1 s confirm that acetone exhibits slow exchange between "in-pore" and "ex-pore" environments.

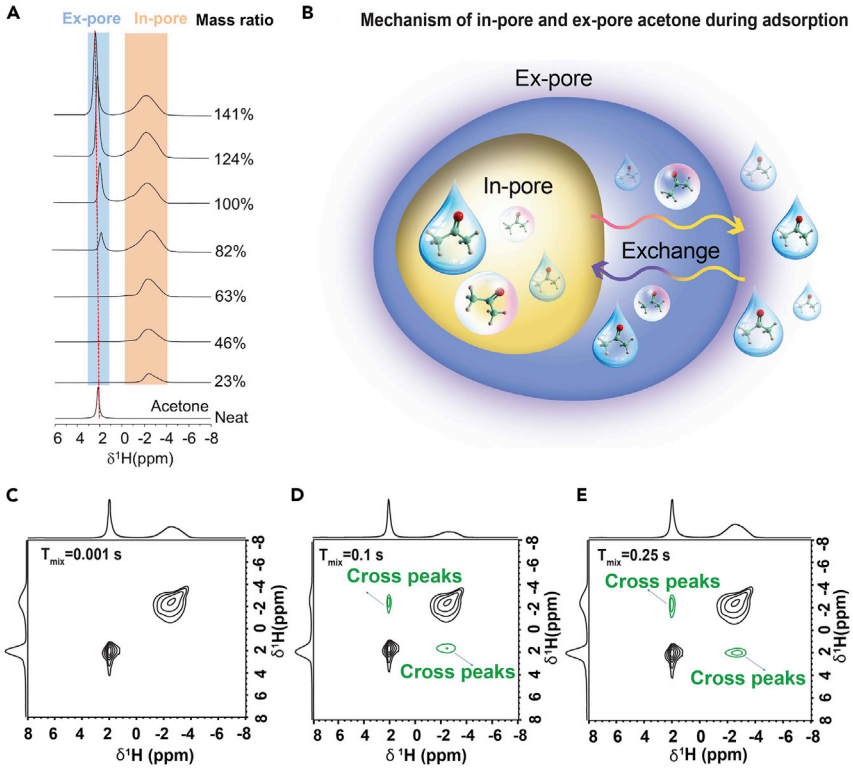

Figure 2. Adsorption of Liquid Acetone in HNC via NMR

(A) ^{1}H NMR spectra of acetone adsorbed onto HNC as a function of loading. The mass ratio is the (mass of acetone used/mass of hierarchical porous nanocarbon material).

(B) Scheme of the local environments of acetone molecules in HNC, including in-pore, ex-pore, and exchange species.

(C–E) Two-dimensional ^{1}H homonuclear correlation experiments. Experiments were performed on a sample with 100% mass ratio of (acetone/HNC), with mixing times of (C) 0.001 s, (D) 0.1 s, and (E) 0.25 s. The cross peaks appearing at mixing times of 0.1 and 0.25 s demonstrate slow exchange between in-pore and ex-pore environments.

Adsorption of Liquid Toluene and *n*-Hexane in Hierarchical Nanoporous Carbons

As shown in Figure S2, we obtained the ^{1}H spin-echo MAS spectra of toluene and *n*-hexane adsorbed onto HNC as a function of loading. The qualitative features of these spectra are analogous to those observed from acetone; the methyl and aromatic proton resonances from toluene reveal in-pore and ex-pore environments, as do the CH_3 and CH_2 resonances from *n*-hexane. At a mass ratio of 62 wt %, the pores of HNC become "full" and the toluene/*n*-hexane loading reaches saturation. As the loading increases, the narrow lines emanating from ex-pore features become prominent. Therefore, the four peaks at low and high frequencies are assigned to in-pore and ex-pore toluene, respectively (Figure S2A). For these adsorbates, we calculate $\Delta\delta$ to be −4.2 ppm (acetone), −4.2 ppm (toluene), and −4.4 ppm (both CH_3 and CH_2 resonances from *n*-hexane) (Figure S2B). The chemical-shift deviations $\Delta\delta$ are very similar for the three adsorbates, indicating that the underlying mechanism is mainly due to ring-current shifts associated with the aromatic rings in the HNC.

Comparison of Uptakes between NMR Spectra and Adsorption Isotherms

Quantitative NMR spectroscopy can be used to provide an alternative method to provide adsorption uptakes.[43] The adsorption isotherms of acetone/toluene/*n*-hexane for our HNC were acquired using a sorption analyzer at 298 K with N_2 as the

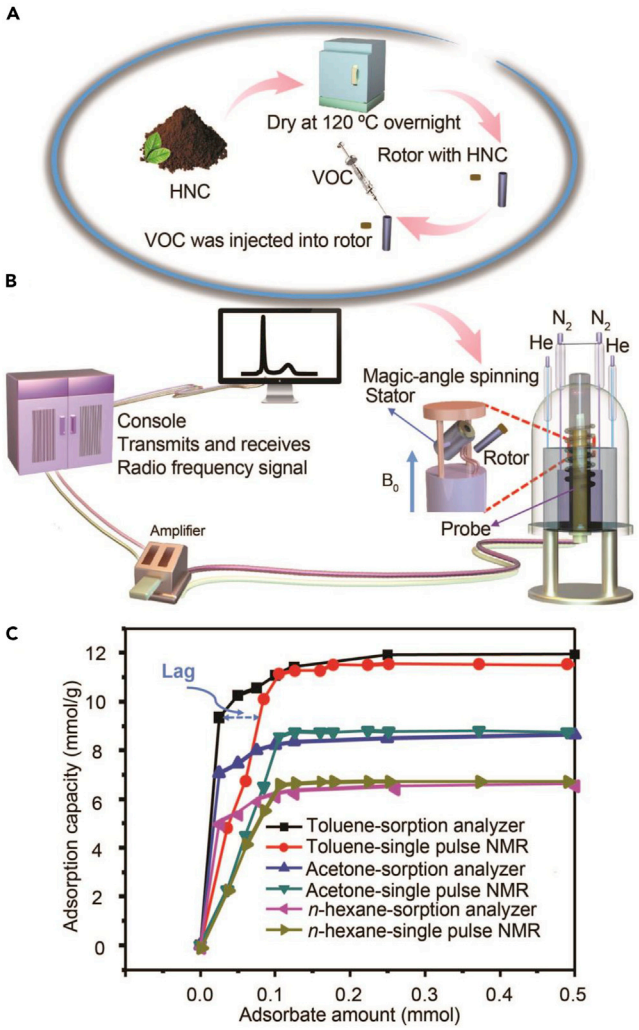

Figure 3. Uptakes of NMR and Gas-Sorption Data

(A) Schematic of the liquid VOC adsorption process.

(B) Schematic of the solid-state NMR measurements of liquid VOC-loaded HNC.

(C) Comparison of uptakes between NMR data and gas-sorption analyzer data for acetone-, toluene-, and *n*-hexane-loaded HNC at room temperature (~298 K). NMR data corroborate the ultimate adsorption capacity but lag the isotherm data at low loadings.

carrier gas, shown in Figure 3C. The proton (^{1}H) single-pulse NMR spectra of liquid acetone, toluene, and *n*-hexane spectra adsorbed at various loadings were deconvoluted and integrated using dmfit software (Figure S3),[44] thus providing the amount (in mmol) of adsorbed in-pore VOC per gram of HNC (Figure 3C). For comparison of NMR uptake with gas-sorption studies, the abscissa is given as mmol of VOC adsorbed. For the NMR data, this is the amount of liquid VOC placed into the sample; for the isotherm data, this is determined by converting the partial pressure (P/P_0) to mmol via the Peng-Robinson equation of state.[45] The result shows that the ultimate uptakes of adsorbates, as measured from adsorption isotherms, are in good agreement with those determined from the NMR spectra. The reason for the lag at low uptakes is unclear and requires further study.

The adsorption capacity of the three compounds within the HNC was found to be in the order of toluene > acetone > *n*-hexane. This order of adsorption capacity clearly

demonstrates the effects of the molecular dimension and polarity of these three VOCs.[41,46] By way of comparison with the HNC synthesized in this work, VOC isotherms and adsorbate capacity on commercial activated carbon were also performed. Our HNC exhibit higher adsorption capacities for all VOCs compared with commercial activated carbon (Figure S4). The saturated toluene, acetone, and *n*-hexane adsorption capacities reached 11.9, 8.8, and 7.2 mmol/g, respectively, which are 1.5-, 1.6-, and 1.9-fold higher than those of commercial activated carbon, respectively. Consequently, our HNC demonstrate high adsorptive performance of VOCs, providing a cost-effective alternative to commercial activated carbon in many air-quality remediation and treatment applications.

VOC Vapor Adsorption in Hierarchical Nanoporous Carbons

In many practical applications, VOC adsorption occurs from the vapor phase rather than the liquid phase, whereby the time required for adsorbents to equilibrate with dosed gas has significance for process swing designs. Therefore, we further examined vapor VOCs loaded onto HNC as a function of adsorption time. Figure 4B depicts the ^{1}H NMR spectra of acetone vapor adsorbed onto HNC as a function of adsorption time at room temperature. After exposure to acetone vapor (Figure 4B) for 1 min, we observed a broad peak at −0.4 ppm (labeled "A"). With increasing adsorption time to 91 min, the intensity of peak A gradually decreases, ultimately disappearing after 150 min. A second upfield peak (~2.5 ppm, peak B) increases to a maximum intensity, suggesting a saturation of the micropores. Figure 4D confirms that the total proton NMR signal, which is integrated from the "within-pore" environments (both peak A and peak B), changes as a function of adsorption time, where, as expected, the adsorption uptake increases with time and reaches saturation at ~91 min. Compared with the liquid-phase loaded HNC spectrum (Figure 4A), the ex-pore peak at ~2 ppm does not appear, indicating that all the gas molecules enter the pores, and no extra molecules remain exterior to the pores.

Noting that adsorbate molecules in smaller pores experience a greater average degree of ring-current shielding—and thus demonstrate a greater shift to low frequency than those in larger pores[30]—the more negative chemical shift for peak B suggests that these acetone molecules are adsorbed in smaller pores vis-à-vis those corresponding to peak A. We consider two hypotheses to explain the NMR spectra, shown in Figures 4C–4F. First, the diffusion of acetone within the HNC pore network over time could change the observed NMR shifts as the adsorbate molecules diffuse to different carbon-pore environments (Figure 4F). To test this hypothesis, we performed a ^{1}H NMR experiment in which HNC were exposed to acetone vapor was for 1 min, followed by a further 3 h of exposure to argon gas for diffusion/equilibration. Figure S5 shows that, after waiting for 3 h, the chemical shift of the spectrum is not changed. Additionally, we conducted a ^{1}H NMR experiment where acetone vapor was exposed to HNC for 1 min, followed by heating the acetone-adsorbed samples to 55°C for 30 min and then cooling them down to room temperature. Figure S6 shows that the chemical shift of the spectrum is unchanged after the treatment. In brief, once adsorbed with an initial aliquot of vapor in site A, neither time nor temperature induced site B occupancy. The temporal progression in Figure 4B, whereby the NMR peak associated with site A decreases and the peak associated with site B increases with time, suggests that acetone distribution between these sites requires continuous exposure to acetone vapor.

A second hypothesis is that thermodynamic effects are responsible for the persistence of site-A occupancy with time and temperature. Schroeder's paradox,[32] whereby adsorption of saturated vapor differs from that exposed to liquid, has

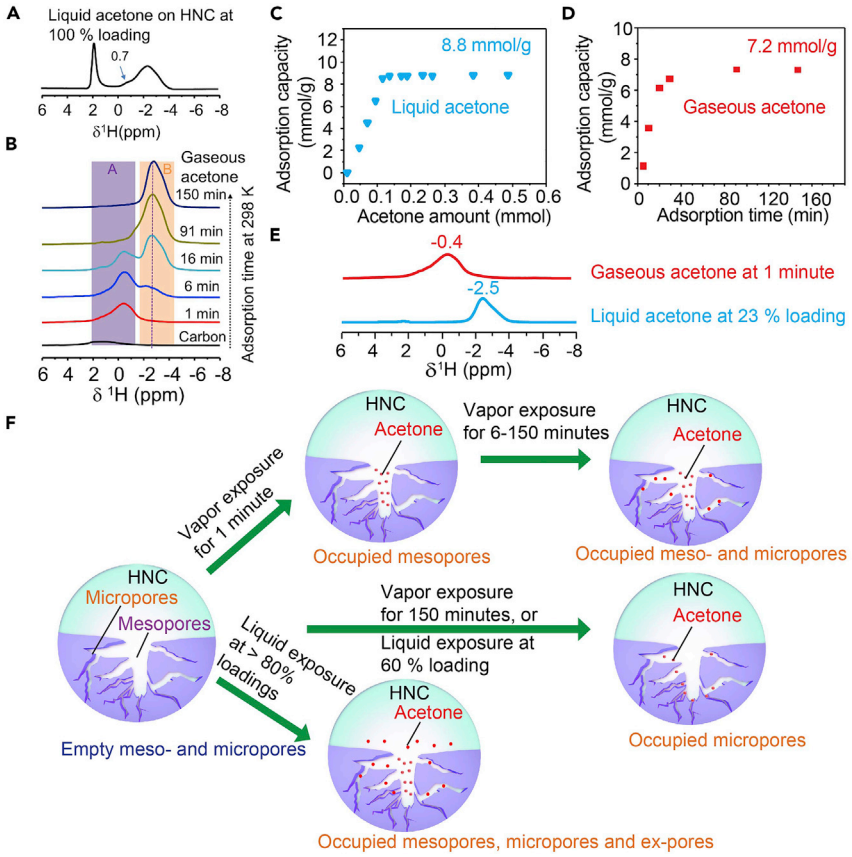

Figure 4. Acetone Adsorption Mechanism and Manifestation of Schroeder's Paradox onto HNC

(A) ^{1}H NMR spectra of liquid acetone at 100 wt % loading shown as a comparison.

(B) ^{1}H NMR spectra of vapor acetone subject to HNC at various adsorption times at ~298 K.

(C) Liquid acetone adsorption capacity at 141 wt %.

(D) Adsorption capacity ("A" + "B" in panel B) changes with increase of adsorption time and reaches saturation over 91 min.

(E) NMR spectra of liquid and gaseous acetone with different chemical shifts.

(F) Adsorbate molecule diffusion to different HNC environments.

been discussed extensively in the literature.[47,48] For example, Schroeder's paradox occurs in strongly interacting systems, in which the materials undergo a high degree of swelling.[48] The data shown in Figure 4E suggest that the distribution of acetone in HNC mesopores depends on the way in which the adsorbate was introduced: an initial aliquot from the vapor yields a peak with a shift of −0.4 ppm, whereas initial exposure to liquid acetone yields a peak at −2.5 ppm (Table S2 displays spectral simulation parameters obtained from deconvolution using dmfit software). In Table S3, we summarize the adsorption capacities of HNC for all VOCs after liquid and vapor exposure. It is clear that the adsorption capacity of saturated VOCs within the HNC is quite different between saturated liquid and vapor VOC; for example, the adsorption capacity of 7.2 mmol/g for acetone vapor with exposure time of 150 min is different from that of liquid acetone with 8.8 mmol/g at 141 wt % loading (Figures 4C and 4D). This difference of adsorption capacities would seem to be a capacity-probed manifestation of Schroeder's paradox.

The observed chemical shifts of adsorbed acetone from the liquid phase are different from those arising from an initial aliquot of vapor-phase adsorbed acetone

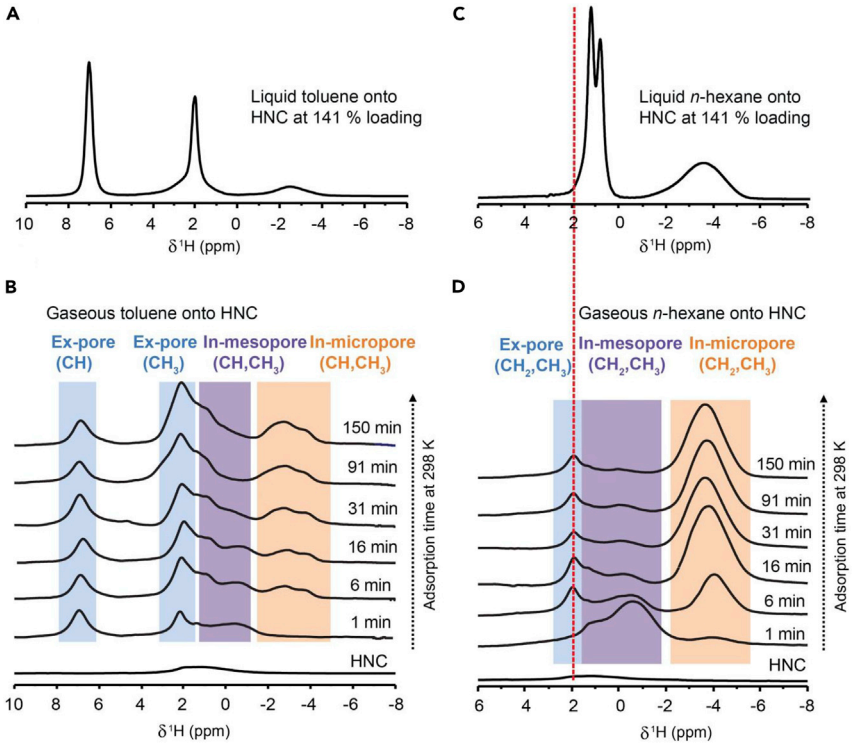

Figure 5. Toluene and *n*-Hexane Vapor Adsorption on Hierarchical Nanoporous Carbons

(A and B) (A) ^{1}H NMR spectra of liquid toluene at 141 wt % loading shown as a comparison and (B) ^{1}H NMR spectra of toluene vapor subject to HNC as a function of adsorption time.

(C and D) (C) ^{1}H NMR spectra of liquid *n*-hexane at 141 wt % loading shown as a comparison and (D) ^{1}H NMR spectra of *n*-hexane vapor subject to HNC as a function of adsorption time.

(Figure 4E). The reason might be that the acetone vapor diffuses into the pore structure in a process different from that of liquid acetone. A comparison of effective liquid and vapor diffusion time (Figures 2A and 4B) in HNC reveals that acetone vapor requires continuous exposure for a long period (150 min) to redistribute from mesopores (site A) to microporous environments (site B). This is confirmed by the large NICS (nucleus-independent chemical shift) value obtained at long exposure. At 16 min of exposure, two peaks are clearly present, revealing that acetone in mesopores and micropores does not undergo exchange on the NMR timescale, thus indicating slow diffusion in HNC under continuous vapor exposure (Figures 2D and 2E). However, liquid acetone diffuses immediately into the micropores (Figure 2A, 23 wt %) and fills the mesopores at higher loading (Figure 2A, 63 wt %). The detailed scheme of the illustration of liquid and gaseous acetone diffusion is shown in Figure 4F.

Figure 5A presents the ^{1}H NMR spectra of HNC subjected to vapor-phase toluene as a function of adsorption time. After toluene exposure for 1 min, several peaks appeared. Those with the largest shifts are easily assigned to ex-pore aromatic and ex-pore methyl protons, owing to the similarity of their shifts to those of neat toluene. This is consistent with a picture in which some toluene molecules cannot go into the pores after short exposure times because the molecular size of toluene is larger than that of the narrow pores in the HNC. The assignment of the upfield shifted proton peaks is not clear, yet the shifts suggest ring-current effects, and we thus assign them to in-mesopore (C–H) and in-mesopore CH_3, as indicated in

Figure 5B (the spectrum at 1 min). With an increase in adsorption time (150 min), the two broad peaks at 1.28 and −0.68 ppm shift further upfield (i.e., lower chemical-shift values) to −2.74 and −3.85 ppm. Again, the increased ring-current effects are the likely cause, and we thus assign these peaks to the in-micropore (C–H) and in-micropore (CH_3), respectively. Interestingly, for the spectrum of vapor-adsorbed HNC at 150 min, the signal at 0.88 ppm assigned to in-mesopore (C–H) environments does not move to a lower chemical shift, indicating that there are toluene molecules still adsorbed in the mesopore due to the larger molecule size of toluene, as compared with the narrow pore size of HNC. Compared with the liquid adsorption spectrum at 141 wt % toluene (Figure 5A), the vapor spectra provide more subtle information about the interactions in different pores as a function of adsorption time. As in the case of acetone, it would appear that Schroeder's paradox is at play.

The ^{1}H NMR spectra obtained for *n*-hexane vapor within the HNC as a function of adsorption time are shown in Figure 5D. With the initial exposure to *n*-hexane for 1 min, ^{1}H MAS NMR signals of the in-mesopore (CH_2) and in-mesopore (CH_3) molecules in the range of ∼2 to ∼−2 ppm overlap, while the broad peak at −3.94 ppm emerges and is assigned to the in-micropore (CH_2 and CH_3) environments. At 6 min, the sharp peak at 1.98 pm is assigned to the overlap of two environments corresponding to ex-pore (CH_2) and ex-pore (CH_3). With increasing adsorption time, as expected, in-mesopore (CH_2) and in-mesopore (CH_3) signals diminish, while those at −3.71 ppm attributed to the in-micropore (CH_2 and CH_3) increase. It is interesting to note that the chemical-shift difference ($\Delta\delta$ = 0.6 ppm) between ex-pore *n*-hexane vapor and ex-pore liquid *n*-hexane peaks (Figure 5C) is probably due to a small amount of chemical exchange between the ex-pore and in-pore gas species, which shifts the chemical shift of the ex-pore vapor away from the ex-pore liquid.[31] As also observed with acetone and toluene, the nature of pore occupancy by the adsorbate depends on whether the sample is exposed to saturated vapor or liquid.

CO_2 Capture Performance

Figure 6A shows the CO_2 adsorption isotherms for HNC at 298 K and 1 bar. Remarkably, it can be found that our HNC exhibited a high CO_2 adsorption capacity of 4.3 mmol/g, thereby reflecting a strongly competitive CO_2 adsorption capacity among the other porous framework materials (e.g., 3.78 mmol/g for rice husk-derived activated carbons at 298 K and 1 bar;[49] for comparison, the capacity of MOF-74 at 298 K and 1 bar[50] is 4.1 mmol/g). The ^{13}C MAS NMR spectra of $^{13}CO_2$-dosed HNC exhibit resonances that were assigned to physisorbed CO_2 at 121.7 ppm (Figure 6C). A similar peak at 124.7 ppm was observed in MOF-274.[44] The −6 ppm chemical shift vis-à-vis free gas-phase CO_2 (127.7 ppm at 1 bar) is due to aromatic ring currents.[51] Therefore, our HNC has excellent CO_2 capacity that, combined with the inexpensive, sustainable, facile, and up-scalable synthesis method, warrants further study with potential application toward carbon-capture technologies.

Conclusions

In summary, we prepared HNC from pinewood that exhibit multi-branching micro- and mesopores and follow Murray's law. These HNC exhibit a large surface area (2,765 m^2/g) and micropore volume (0.741 cc/g), which portends a potentially important role in the adsorption of gases. We probed the adsorption of VOCs at the molecular level via ^{1}H MAS NMR. Acetone, toluene, and *n*-hexane were found to exhibit NMR spectra that quantify the mass of adsorbate, and changes of the adsorbate spectra with time were seen after exposure to the HNC. Liquid acetone, toluene, and *n*-hexane present broad NMR signals that are shifted to lower frequency; these peaks are assigned to in-pore adsorbed VOCs where the shift is

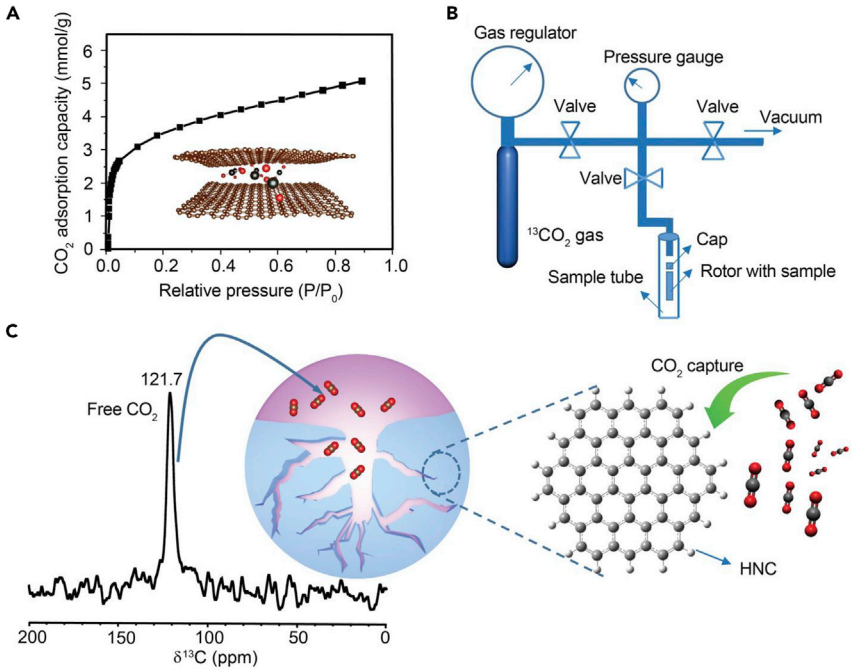

Figure 6. CO_2 Adsorption on Hierarchical Nanoporous Carbon

(A) CO_2 adsorption isotherm onto HNC at 298 K and 1 bar; adsorption isotherm samples were activated under N_2 at 120°C for 2 h, followed by activation under vacuum at 120°C for 4 h.

(B) Schematic of setup for $^{13}CO_2$ gas dosing into NMR samples.

(C) ^{13}C NMR spectra by direct excitation (no ^1H decoupling) on $^{13}CO_2$-loaded HNC at 755 mbar.

attributable to the ring currents arising from the graphene-like sheets. In addition, narrow signals appear at the same chemical shift as those from the neat liquid VOCs. These latter peaks appear only at high loadings, consistent with pore saturation. In the case of acetone adsorption at high loadings, the adsorbate undergoes slow (~0.1 s) exchange between in-pore and ex-pore environments. Uptakes determined from ^1H NMR are obtained by calibrating the signal at various loadings and are consistent with that of gas-sorption analyzer data at saturation coverages, showing that NMR allows for fast determination of the ultimate adsorption capacities of VOCs within the HNC. Regarding gaseous adsorption, ^1H NMR spectra of vapor-adsorbed VOCs into HNC as a function of exposure time showed that VOCs occupy initial mesopores and finally micropores. By comparison with liquid adsorption, we proposed that the data are consistent with an observation of Schroeder's paradox. In the case of gas-phase uptake of CO_2, we find that the HNC show high physisorption of CO_2 (4.3 mmol/g), which is consistent with potential application to carbon-capture technologies. We conclude that the synthesis of HNC—and the NMR-determined pore distribution of adsorbates with loading and time—portend the observation of both new phenomena and novel technological applications in the multidisciplinary field of energy, environment, and economics.

EXPERIMENTAL PROCEDURES

Resource Availability

Lead Contact

Further information and requests for resources and reagents should be directed to and will be fulfilled by the Lead Contacts, Jeffrey A. Reimer (Reimer reimer@berkeley.edu) and Yi Cui (yicui@stanford.edu).

Materials Availability

This study did not generate new unique reagents.

Data and Code Availability

The data that support the plots within this paper and other findings of this study are available from the corresponding authors on request.

Synthesis of Hierarchical Nanoporous Carbons

The pinewood chips were thoroughly washed and placed into a muffle furnace prior to carbonization. The carbonization temperature was 600°C under a purified N_2 flow (0.5 L/min). After carbonization, the char was sieved to obtain particles of 1–2 mm in diameter. The char produced was mixed with K_2CO_3 with an impregnation K_2CO_3/char mass ratio of 3.0. The mixture was heated in a modified 2.45-GHz microwave oven with an output power of 700 W for 20 min, with humidified N_2 as the carrier gas. The resultant hierarchical nanoporous carbon was washed with 0.1 M hydrochloric acid and repeatedly rinsed with hot and cold distilled water to remove residual K from the sample's surface until the filtrate reached neutral pH. The experimental setup is shown in Figure 1A. Additionally, to provide a comparison with the as-synthesized HNC, commercial activated carbons were obtained from EM Industries and characterized in tandem as described below.

Sample Characterization

SEM images were acquired on a Hitachi S-2500 (Tokyo, Japan) analytical scanning electron microscope using beam energy of 20 kV and an In-Lens detector. TEM images were acquired on a ThemIS microscope (TEM 0.5) at 300 kV. The specific surface area and pore structure of the samples were evaluated using a Micromeritics ASAP2010 physical adsorption instrument at 77 K in liquid argon. The specific surface area was estimated by the BET method.[25] The pore-size distribution for micropores was calculated using the *t*-plot method.

Preparation of Samples in NMR Rotors for Adsorption Experiment

The schematic of the preparation of samples is depicted in Figure 3A. The samples used here were ground into powder (fine mesh) and placed into a vacuum oven at 120°C overnight, then packed into 4-mm sealing cells, which were subsequently put into zirconia MAS rotors (4 mm outer diameter). Sealing cells were weighed prior to and after packing to determine the mass of the HNC. For liquid VOCs, a microsyringe was used to inject solvents (acetone [Sigma, 99%], toluene [Sigma, 99.9%], and *n*-hexane [Sigma, *n*-hexane 98.5%]) into the sealing cell. The samples were subjected to NMR analysis 24 h after adsorption to reach the adsorption equilibrium. The aforementioned adsorption experiment was performed in a glovebox with argon gas to avoid the effects of moisture. The following mass balance equation was used to determine the mass of VOCs injected into HNC:

$$W = \frac{W_2 - W_1}{W_1} \times 100\%, \qquad \text{(Equation 1)}$$

where W is the mass of VOCs normalized by the mass of the hierarchical nanoporous carbon material, W_2 is the weight of the HNC after adding VOCs, and W_1 is the weight of the HNC. Neat solvent experiments were performed on a mixture of KBr and pure VOCs in the sealing cell to ensure rotor stability during NMR. For gaseous adsorption, VOC solvents and the rotor with HNC were placed in separate scintillation vials and then placed in a sealed vial; further details are given below and in Figure 3A. Adsorption isotherms were measured by using the gas adsorption analyzer. After adsorption, the inserts with liquid/vapor VOC-adsorbed HNC were transferred into a vacuum oven at 120°C, left overnight, and stored in a desiccator for future use.

Prior to CO_2 adsorption, HNC samples were packed into a 3.2-mm rotor under a nitrogen environment to avoid moisture. The rotor containing samples was then put into a home-built gas setup (Figure 6B).[44] Before dosing with $^{13}CO_2$ gas (Sigma-Aldrich, 99 atom % ^{13}C, <3 atom % ^{18}O), the samples were evacuated for 10 min. $^{13}CO_2$ dosing was carried out overnight to reach equilibration at room temperature (~298 K). Meanwhile, a gas gauge was used to control and record the pressure inside the samples. After adsorption, the rotor was sealed by the cap using a moveable plunger inside the setup to avoid air and moisture.

NMR Experiments

The schematic depicting the NMR experiments is shown in Figure 3B. The ^1H MAS NMR spectra were measured at 500.12 MHz (11.7 T) on a Bruker Avance spectrometer with a Bruker narrow-bore H/C/N MAS probe. The ^1H MAS one-pulse NMR spectra of VOCs adsorbed in HNC was acquired at a sample spinning rate of 8 kHz. Neat VOCs with KBr were spun at 5 kHz. To eliminate the background signal from the NMR probe, we used both spin-echo (90°-τ-180°-τ-acquire) and one-pulse sequence measurements to record the ^1H spectra.[52] A radiofrequency field strength (B_1) of 60 kHz and a spin-echo delay of τ = 119 μs were used, while using a recycle delay of 1 s. ^1H two-dimensional homonuclear exchange experiments were performed on samples with VOC loadings where additional peaks (relative to the neat VOCs) emerged.[53] Mixing times in the range of 0.001, 0.1, and 0.25 s were used. For CO_2 adsorption experiments, the NMR experiment was performed at 16.4 T using a Bruker 3.2-mm MAS probe with an MAS rate of 15 kHz. ^{13}C NMR spectra by direct excitation were measured in the CO_2 adsorption experiment. The proton and ^{13}C peaks of adamantane at 1.85 and 38.5 (tertiary carbon high-frequency resonance) ppm, respectively, were used as an external reference. All NMR experiments were performed at ambient temperature (~298 K). Spectral fitting was carried out using dmfit software. Deconvolutions were calculated using a mixture of Gaussian and Lorentzian lineshapes to describe the different features in the spectra.

The ^1H MAS one-pulse NMR spectra of vapor VOCs adsorbed in HNC were also acquired at a sample spinning rate of 8 kHz. The schematic of vapor adsorption in HNC is shown in Figure S7. HNC were packed into a 4-mm rotor in an argon glovebox. VOC solvents and a rotor with HNC were placed in separate scintillation vials, both of which were placed in a parafilm-sealed beaker. To minimize moisture adsorption, we put this sealed beaker in a glovebox for various adsorption times. After a specified adsorption time (e.g., 1 min), the rotor was capped in the glovebox and transferred to the NMR spectrometer.

To assess the diffusion of acetone within the mesopores of the HNC, we exposed acetone vapor to HNC for 1 min in the sealed beaker, after which the rotor was quickly capped and placed in an argon glovebox for 3 h. Additional ^1H NMR experiments were carried out, as shown in Figure S5. Prior to exposing acetone vapor to HNC for 1 min, argon gas was introduced into the glovebox, followed by evacuation for 2 h. After that, the rotor cap was quickly inserted and sealed, and the sample was heated to 55°C for 30 min in an oven. After cooling to room temperature, a one-pulse MAS NMR experiment was performed.

Adsorption Isotherm Experiments

The adsorption isotherms were performed gravimetrically using a sorption analyzer (TA Instruments, model VTI-SA) at 298 K with N_2 as the carrier gas. The system recorded the equilibrium weight of the biomass-based HNC in response to a step-change in the concentration of the adsorbate (relative pressure range of 0.01–0.9). Between 3 and 5 mg of HNC powder was weighed and placed into the container

of the analyzer. Equilibrium was assumed to be reached when the weight changed by less than 0.001% in a 5-min period.

SUPPLEMENTAL INFORMATION

Supplemental Information can be found online at https://doi.org/10.1016/j.matt.2020.09.024.

ACKNOWLEDGMENTS

This work was supported as part of the Center for Gas Separations Relevant to Clean Energy Technologies, an Energy Frontier Research Center funded by the US government. This work was supported by the Department of Energy, Office of Basic Energy Sciences, Division of Materials Sciences and Engineering (contract no. DE-AC02-76SF00515). D.M.H. acknowledges support from the Joint Center for Energy Storage Research, an Energy Innovation Hub funded by the US Department of Energy, Office of Science, Basic Energy Sciences. We appreciate technical discussions with Dr. Alexander C. Forse and Dr. Thomas M. Osborn Popp.

AUTHOR CONTRIBUTIONS

Y.C., J.A.R., J.T., and H.M. conceived the idea and composed the manuscript. H.M. and J.T. planned the study, designed the experiment, and analyzed the data. H.M. and J.T. performed all the experiments . Y.C. and J.A.R. supervised the project. All of the authors reviewed and commented on the manuscript.

DECLARATION OF INTERESTS

The authors declare no competing interests.

Received: July 29, 2020
Revised: August 25, 2020
Accepted: September 28, 2020
Published: October 22, 2020

REFERENCES

1. Brüggemann, M., Hayeck, N., and George, C. (2018). Interfacial photochemistry at the ocean surface is a global source of organic vapors and aerosols. Nat. Commun. *9*, 2101.

2. Boyd, P.G., Chidambaram, A., García-Díez, E., Ireland, C.P., Daff, T.D., Bounds, R., Gładysiak, A., Schouwink, P., Moosavi, S.M., Maroto-Valer, M.M., et al. (2019). Data-driven design of metal–organic frameworks for wet flue gas CO_2 capture. Nature *576*, 253–256.

3. Chen, W.Y., Jiang, X., Lai, S., Peroulis, D., and Stanciu, L. (2020). Nanohybrids of a MXene and transition metal dichalcogenide for selective detection of volatile organic compounds. Nat. Commun. *11*, 1302.

4. Dong, J., and Zhang, K. (2017). Ultrathin two-dimensional porous organic nanosheets with molecular rotors for chemical sensing. Nat. Commun. *8*, 1142.

5. Chen, W., Chen, S., Liang, T., Zhang, Q., Fan, Z., Yin, H., Huang, K., Zhang, X., Lai, Z., and Sheng, P. (2018). High-flux water desalination with interfacial salt sieving effect in nanoporous carbon composite membranes. Nat. Nanotechnol. *13*, 345–350.

6. McDonald, T.M., Mason, J.A., Kong, X., Bloch, E.D., Gygi, D., Dani, A., Crocella, V., Giordanino, F., Odoh, S.O., Drisdell, W.S., et al. (2015). Cooperative insertion of CO_2 in diamine-appended metal-organic frameworks. Nature *519*, 303–308.

7. Joo, W.J., Lee, J.H., Jang, Y., Kang, S.G., Kwon, Y.N., Chung, J., Lee, S., Kim, C., Kim, T.H., Yang, C.W., et al. (2017). Realization of continuous Zachariasen carbon monolayer. Sci. Adv. *3*, e1601821.

8. Yadavalli, T., Ames, J., Agelidis, A., Suryawanshi, R., and Jaishankar, D. (2019). Drug-encapsulated carbon (DECON): a novel platform for enhanced drug delivery. Sci. Adv. *5*, eaax0780.

9. Xu, L., Li, Y., Gao, S., Niu, Y., Liu, H., Mei, C., Cai, J., and Xu, C. (2020). Preparation and properties of cyanobacteria-based carbon quantum dots/polyvinyl alcohol/nanocellulose composite. Polymers (Basel) *12*, 1143.

10. Yu, D., Goh, K., Wang, H., Wei, L., Jiang, W., Zhang, Q., Dai, L., and Chen, Y. (2014). Scalable synthesis of hierarchically structured carbon nanotube-graphene fibres for capacitive energy storage. Nat. Nanotechnol. *9*, 555–562.

11. Tseng, P., Napier, B., Zhao, S., Mitropoulos, A.N., Applegate, M.B., Marelli, B., Kaplan, D.L., and Omenetto, F.G. (2017). Directed assembly of bio-inspired hierarchical materials with controlled nanofibrillar architectures. Nat. Nanotechnol. *12*, 474–480.

12. Abraham, J., Vasu, K.S., Williams, C.D., Gopinadhan, K., Su, Y., Cherian, T.C., Dix, J., Prestat, E., Haigh, S.J., Grigorieva, I.V., and Carbone, P. (2017). Tunable sieving of ions using graphene oxide membranes. Nat. Nanotechnol. *12*, 546–550.

13. Wu, J., Wu, J., Xu, F., Li, S., Ma, P., Zhang, X., Liu, Q., Fu, R., and Wu, D. (2019). Porous polymers as multifunctional material platforms toward task-specific applications. Adv. Mater. *31*, 1802922.

14. Wang, H., Min, S., Ma, C., Liu, Z., Zhang, W., Wang, Q., Li, D., Li, Y., Turner, S., Han, Y., et al. (2017). Synthesis of single-crystal-like nanoporous carbon membranes and their application in overall water splitting. Nat. Commun. *8*, 13592.

15. Jessen, B.S., Gammelgaard, L., Thomsen, M.R., Mackenzie, D.M.A., Thomsen, J.D., Caridad, J.M., Duegaard, E., Watanabe, K., Taniguchi,

T., Booth, T.J., et al. (2019). Lithographic band structure engineering of graphene. Nat. Nanotechnol. *14*, 340–346.

16. Xia, H., Tang, H., Zhou, B., Li, Y., Zhang, X., Shi, Z., Deng, L., Song, R., Li, L., Zhang, Z., et al. (2020). Mediator-free electron-transfer on patternable hierarchical meso/macro porous bienzyme interface for highly-sensitive sweat glucose and surface electromyography monitoring. Sensors Actuators B Chem. *312*, 12792.

17. Lin, X., Liang, Y., Lu, Z., Lou, H., Zhang, X., Liu, S., Zheng, B., Liu, R., Fu, R., and Wu, D. (2017). Mechanochemistry: a green, activation-free and top-down strategy to high-surface-area carbon materials. ACS Sustain. Chem. Eng. *5*, 8535–8540.

18. Du, Y., Huang, Z., Wu, S.K., Xiong, X., Zhang, Zheng, B., Nadimicherla, R., Fu, R., and Wu, D. (2018). Preparation of versatile yolk-shell nanoparticles with a precious metal yolk and a microporous polymer shell for high-performance catalysts and antibacterial agents. Polymer *137*, 195–200.

19. Zheng, X., Shen, G., Wang, C., Li, Y., Dunphy, D., Hasan, T., Brinker, C.J., and Su, B. (2017). Bio-inspired Murray materials for mass transfer and activity. Nat. Commun. *8*, 14921.

20. Wang, X., Wang, X., Huang, Z., Miao, D., Miao, D., Zhao, J., Yu, J., and Ding, B. (2018). Biomimetic fibrous Murray membranes with ultrafast water transport and evaporation for smart moisture-wicking fabrics. ACS Nano *13*, 1060–1070.

21. Adinata, D., Wan Daud, W.M.A., and Aroua, M.K. (2007). Preparation and characterization of activated carbon from palm shell by chemical activation with K_2CO_3. Bioresour. Technol. *98*, 145–149.

22. Dahal, N., García, S., Zhou, J., and Humphrey, S.M. (2012). Beneficial effects of microwave-assisted heating versus conventional heating in noble metal nanoparticle synthesis. ACS Nano *6*, 9433–9446.

23. Wang, H., Jahandar Lashaki, M., Fayaz, M., Hashisho, Z., Philips, J.H., Anderson, J.E., and Nichols, M. (2012). Adsorption and desorption of mixtures of organic vapors on beaded activated carbon. Environ. Sci. Technol. *46*, 8341–8350.

24. Lashaki, M.J., Jahandar Lashaki, M., Fayaz, M., Wang, H., Hashisho, Z., Philips, J.H., Anderson, J.E., and Nichols, M. (2012). Effect of adsorption and regeneration temperature on irreversible adsorption of organic vapors on beaded activated carbon. Environ. Sci. Technol. *46*, 4083–4090.

25. Brunauer, S., Emmett, P.H., and Teller, E. (1938). Adsorption of gases in multimolecular layers. J. Am. Chem. Soc. *60*, 309–319.

26. Jahandar Lashaki, M., Atkinson, J.D., Hashisho, Z., Phillips, J.H., Anderson, J.E., and Nichols, M. (2016). The role of beaded activated carbon's surface oxygen groups on irreversible adsorption of organic vapors. J. Hazard. Mater. *317*, 284–294.

27. Pel, L., Valckenborg, R.M.E., Kopinga, K., Aarden, F.B., and Kerkhof, P.J.A.M. (2003). Nitrobenzene adsorption in activated carbon as observed by NMR. AIChE J. *49*, 232–236.

28. Kong, X., Deng, H., Yan, F., Kim, J., Swisher, J.A., Smit, B., Yaghi, O.M., and Reimer, J.A. (2013). Mapping of functional groups in metal-organic frameworks. Science *341*, 882–886.

29. Forse, A.C., Merlet, C., Allan, P.K., Humphreys, E.K., Griffin, J.M., Aslan, M., Zeiger, M., Presser, V., Gogotsi, Y., and Grey, C.P. (2015). New insights into the structure of nanoporous carbons from NMR, Raman, and pair distribution function analysis. Chem. Mater. *27*, 6848–6857.

30. Deschamps, M., Gilbert, E., Azais, P., Raymundo-Piñero, E., Ammar, M.R., Simon, P., Massiot, D., and Béguin, F. (2013). Exploring electrolyte organization in supercapacitor electrodes with solid-state NMR. Nat. Mater. *12*, 351–358.

31. Hippauf, F., Fulik, N., Hippauf, F., Leistenschneider, D., Paasch, S., Kaskel, S., Brunner, E., and Borchardt, L. (2018). Electrolyte mobility in supercapacitor electrodes—solid state NMR studies on hierarchical and narrow pore sized carbons. Energy Storage Mater. *12*, 183–190.

32. Schroeder, P. (1903). Uber Erstarrungs- und Quellungserscheinungen von Gela-tine. Z. Phys. Chem. *45*, 57.

33. Román, S., Ledesma, B., Sabio, E., González, J.F., and González, C.M. (2016). Production of cost-effective mesoporous materials from prawn shell hydrocarbonization. Nanoscale Res. Lett. *11*, 435.

34. Sun, Y., Wei, J., Wang, Y.S., Yang, G., and Zhang, J.P. (2010). Production of activated carbon by K2CO3 activation treatment of cornstalk lignin and its performance in removing phenol and subsequent bioregeneration. Environ. Technol. *31*, 53–61.

35. Chen, R., Li, L., Liu, Z., Liu, M., Wang, C., Li, H., Ma, W., and Wang, S. (2017). Preparation and characterization of activated carbons from tobacco stem by chemical activation. J. Air Waste Manag. Assoc. *67*, 713–724.

36. Horvath, G., and Kawazoe, K. (1983). Method for the calculation of effective pore size distribution in molecular sieve carbon. J. Chem. Eng. Jpn. *16*, 470.

37. Carrott, P.J.M., Carrott, M.M.L.R., Mourão, P.A.M., and Lima, R.P. (2004). Preparation of activated carbons from cork by physical activation in carbon dioxide. Adsorpt. Sci. Technol. *21*, 669–681.

38. Foo, K.Y., and Hameed, B.H. (2012). Mesoporous activated carbon from wood sawdust by K2CO3 activation using microwave heating. Bioresour. Technol. *111*, 425–432.

39. Forse, A.C., Griffin, J.M., Merlet, C., Carretero-Gonzalez, J., Raji, A.R.O., Trease, N.M., and Grey, C.P. (2017). Direct observation of ion dynamics in supercapacitor electrodes using in situ diffusion NMR spectroscopy. Nat. Energy *2*, 16216.

40. Harris, R.K., Thompson, T.V., Norman, P.R., and Pottage, C. (1996). Adsorption competition onto activated carbon, studied by magic-angle spinning NMR. J. Chem. Soc. Faraday Trans. *92*, 2615–2618.

41. Harris, R.K., Thompson, T.V., Norman, P.R., and Pottage, C. (1999). Phosphorus-31 NMR studies of adsorption onto activated carbon. Carbon N. Y. *37*, 1425–1430.

42. Devautour-vinot, S., Maurin, G., Serre, C., Horcajada, P., Cunha, D.P., Guillerm, V., Costa, E.S., Taulelle, F., and Martineau, C. (2012). Structure and dynamics of the functionalized MOF type UiO-66(Zr): NMR and dielectric relaxation spectroscopies coupled with DFT calculations. Chem. Mater. *24*, 2168–2177.

43. Anderson, R.J., McNicholas, T.P., Kleinhammes, A., Wang, A., Liu, J., and Wu, Y. (2010). NMR Methods for characterizing the pore structures and hydrogen storage properties of microporous carbons. J. Am. Chem. Soc. *132*, 8618–8626.

44. Forse, A.C., Milner, P.J., Lee, J.H., Redfearn, H.N., Oktawiec, J., Siegelman, R.L., Martell, J.D., Dinakar, L.B., Porter-Zasada, Gonzalez, M.I., et al. (2018). Elucidating CO_2 chemisorption in diamine-appended metal-organic frameworks. J. Am. Chem. Soc. *140*, 18016–18031.

45. Valiollahi, S., Kavianpour, B., Raeissi, S., and Moshfeghian, M. (2016). A new Peng-Robinson modification to enhance dew point estimations of natural gases. J. Nat. Gas Sci. Eng. *34*, 1137–1147.

46. Ania, C.O., Cabal, B., Parra, J.B., Arenillas, A., Arias, B., and Pis, J.J. (2008). Naphthalene adsorption on activated carbons using solvents of different polarity. Adsorption *14*, 343–355.

47. Vallieres, C., Winkelmann, D., Roizard, D., Favre, E., Scharfer, P., and Kind, M. (2006). On Schroeder's paradox. J. Memb. Sci. *278*, 357–364.

48. Beers, K.M., Yakovlev, S., Jackson, A., Wang, X., Hexemer, A., Downing, K.H., and Balsara, N.P. (2014). Absence of Schroeder's paradox in a nanostructured block copolymer electrolyte membrane. J. Phys. Chem. B *118*, 6785–6791.

49. Liu, X., Sun, C., Liu, H., Tan, W., Wang, W., and Snape, C. (2019). Developing hierarchically ultra-micro/mesoporous biocarbons for highly selective carbon dioxide adsorption. Chem. Eng. J. *361*, 199–208.

50. Millward, A.R., and Yaghi, O.M. (2005). Metal-organic frameworks with exceptionally high capacity for storage of carbon dioxide at room temperature. J. Am. Chem. Soc. *127*, 17998–17999.

51. Forse, A.C., Griffin, J.M., Presser, V., Gogotsi, Y., and Grey, C.P. (2014). Ring current effects: factors affecting the NMR chemical shift of molecules adsorbed on porous carbons. J. Phys. Chem. C *118*, 7508–7514.

52. Nandy, A., Forse, A.C., Witherspoon, V.J., and Reimer, J.A. (2018). NMR spectroscopy reveals adsorbate binding sites in the metal-organic framework UiO-66(Zr). J. Phys. Chem. C *122*, 8295–8305.

53. Aue, W.P., Bartholdi, E., and Ernst, R.R. (1976). Two-dimensional spectroscopy: application to nuclear magnetic resonance. J. Chem. Phys. *64*, 2229–2246.